A hierarchical framework for cortical and subcortical gray-matter parcellation across rodents, primates, and humans

Siva Venkadesh[a,Ψ], Yuhe Tian[a], Wen-Jieh Linn[b], Jessica Barrios Martinez[a], Harrison Mansour[c], James Cook[c], David J. Schaeffer[b,d], Diego Szczupak[d], Afonso C. Silva[b,d], G Allan Johnson[c], Fang-Cheng Yeh[a,#]

[a] Department of Neurological Surgery, University of Pittsburgh, Pittsburgh, PA, USA.

[b] Department of Bioengineering, University of Pittsburgh, Pittsburgh, PA, USA.

[c] Duke Center for In Vivo Microscopy, Departments of Radiology and Biomedical Engineering, Duke University, Durham, NC, USA.

[d] Department of Neurobiology, University of Pittsburgh, Pittsburgh, PA, USA.

Correspondence:
[Ψ]Siva Venkadesh <siv30@pitt.edu>

[#]Fang-Cheng Yeh <frank.yeh@pitt.edu>

Keywords: cross-species atlas, cortical gray matter, comparative neuroscience, minimal deformation templates

Abstract

Translational neuroscience requires consistent anatomical frameworks to compare brain organization across species despite differences in size and specialization. Existing atlases are species-specific, limiting cross-species analyses. Here we constructed population-averaged minimal deformation templates for rodents, nonhuman primates, and humans, and developed a hierarchical common atlas delineating homologous cortical and subcortical gray matter regions through landmark-guided boundaries and multimodal nonlinear registration. Validation against species-specific atlases confirmed strong regional correspondence and revealed systematic volumetric scaling, with humans showing expanded associative cortices and rodents emphasizing limbic and sensorimotor areas. This freely available atlas provides a unified coordinate system supporting comparative imaging, developmental analyses, and cross-species connectomics, facilitating investigations into conserved and divergent brain organization across species.

1. Introduction:

Translational neuroscience aims to uncover principles of brain organization that are shared across species, as well as those that have evolved for specific lineages. However, achieving this requires consistent definitions of brain regions across different species—a task complicated by substantial differences in brain size, folding, and specialization. Despite rapid advances in neuroimaging and histological mapping, a major obstacle persists: there is a need for standardized anatomical framework for translating brains across species. Most available atlases are species-specific and have been developed independently, often using different criteria for parcellation[1–4], This leads to substantial differences in how homologous regions are defined, which can hinder our ability to determine whether observed similarities or differences in network organization reflect true biological principles or are simply artifacts of methodological variation.

Several initiatives have begun to address this challenge. For example, harmonized human atlases have been developed to reconcile differences across parcellation schemes[4–6], and recent efforts have aligned nonhuman primate parcellations to human cortical surfaces to facilitate cross-species comparisons[7,8]. While these approaches have improved anatomical consistency within or between primates, comparable frameworks that encompass both rodents and primates are still lacking. Furthermore, most existing solutions are based on species-specific surfaces or templates and do not utilize population-averaged minimal deformation templates (MDTs), which are reference spaces created by iteratively averaging multiple individuals to minimize anatomical variability. In humans, the ICBM 2009a templates[9] represent the most widely adopted standard, constructed through population averaging and nonlinear registration to reduce inter-individual anatomical differences. In contrast, atlases for other species often rely on single-subject scans or templates not generated using comparable MDT frameworks, resulting in inconsistencies in spatial alignment and anatomical scaling. This methodological disparity undermines the reliability of volumetric comparisons across species.

To address this gap, we first constructed population-averaged minimal deformation templates (MDTs) for each species to provide a consistent anatomical foundation for cross-species alignment. For humans and marmosets, we adopted existing MDTs from the widely used ICBM2009a templates[9] and the Marmoset Brain Atlas[10], respectively. For mouse, rat, and rhesus macaque, we generated new MDTs using high-resolution MRI and iterative diffeomorphic averaging (Online Methods). Building on these templates, we then delineated a common hierarchical atlas of cortical and subcortical gray matter spanning rodents, nonhuman primates, and humans.

The parcellation framework is organized hierarchically, beginning with an initial Level-0 tissue segmentation (defining major tissue compartments), followed by Level-1 macro-regions (major cortical and subcortical divisions), and Level-2 subdivisions (finer anatomical parcels), with all levels defined by consistent anatomical boundaries and literature-guided homologies. For closely related species (e.g., mouse and rat), parcellations were aligned using multimodal nonlinear spatial registration (see Online Methods), while for more divergent species (e.g., humans and nonhuman primates), boundaries were matched using anatomical landmarks and literature-based homologies. Validation against species-specific atlases confirmed robust overlap across major

divisions, and volumetric analyses revealed systematic scaling relationships among species. By establishing a unified coordinate system that ensures cross-species consistency, the atlas enables direct comparison of cortical and subcortical networks. We have made this atlas freely available to support comparative connectomics and developmental studies, providing a foundational anatomical resource for cross-species neuroscience.

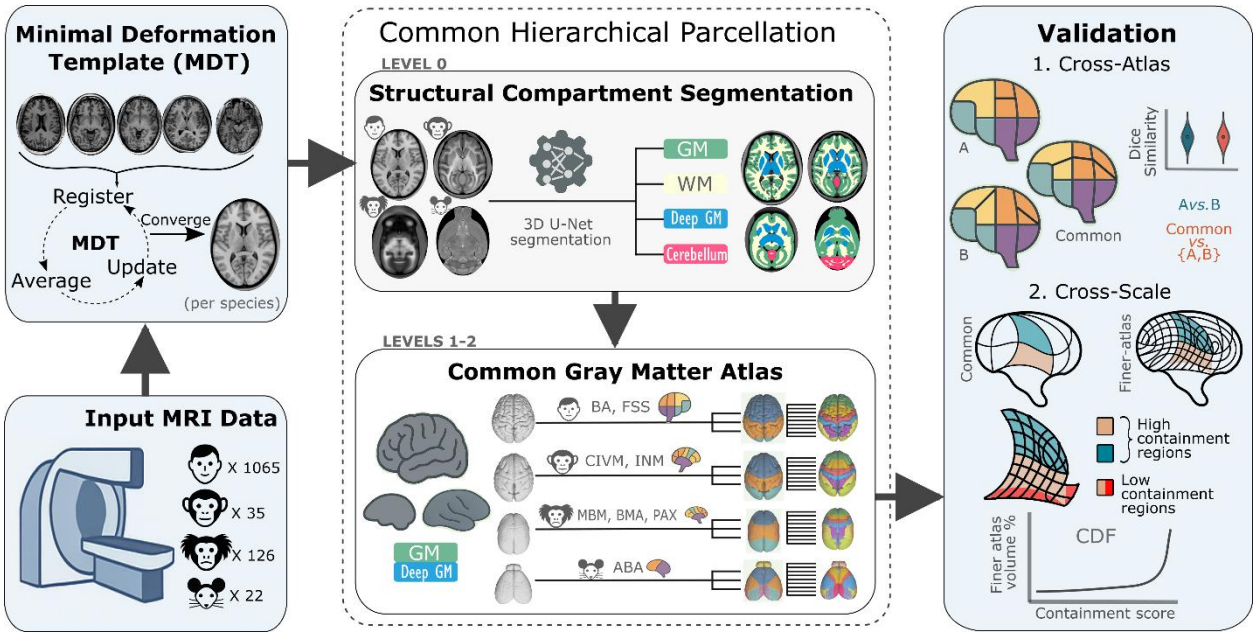

Figure 1 | Overview of the common cross-species atlas framework. The workflow integrates species-specific MRI data into a unified anatomical hierarchy through population-based template construction, automated segmentation, and hierarchical parcellation, validated across scales. **(Left)** *Input MRI data* were acquired for human, rhesus macaque, marmoset, and mouse cohorts. Each species dataset was processed to generate a Minimal Deformation Template (MDT) via iterative diffeomorphic averaging that minimizes anatomical distortion across individuals. **(Center)** On each MDT, Level-0 *structural compartment segmentation* was performed using a 3D U-Net to delineate gray matter (GM), white matter (WM), deep gray matter (Deep GM), and cerebellum. These compartment maps provided the foundation for a *Common Hierarchical Parcellation* spanning Levels 1–2. The Common Gray Matter Atlas was then constructed by harmonizing cortical and subcortical parcels across species using literature-guided anatomical homologies (human – FreeSurferSeg/Brodmann; rhesus – CIVM/INM; marmoset – MBM/BMA/Paxinos; mouse – ABA). **(Right)** *Validation* was performed at two levels: (1) Cross-atlas validation quantified overlap (Dice similarity) between the common atlas and independent species-specific atlases, comparing common vs. others with inter-atlas overlaps (A vs B); (2) Cross-scale containment validation tested how well finer atlas regions from species-specific parcellations were spatially contained within the broader common atlas parcels, quantifying the extent to which the common atlas respects finer-atlas boundaries.

2. Results:

2.1. Overview of the Common Atlas Framework

Figure 1 summarizes the overall workflow for constructing the cross-species common atlas. Input MRI data from human, rhesus macaque, marmoset, and mouse were first used to generate Minimal Deformation Templates (MDTs) through iterative diffeomorphic averaging, similar to ANTs population-template methods[11,12]. The MDT ensures that each species' reference template represents a population-average configuration with minimal anatomical distortion, providing a consistent spatial foundation for inter-species alignment.

Each MDT was then processed using a 3D U-Net segmentation model trained to delineate major tissue classes: gray matter (GM), white matter (WM), deep gray matter (DGM), cerebellum (CBL), and cerebrospinal fluid (CSF). This segmentation defined the Level 0 structural hierarchy, which served as the foundation for all higher-order parcellations. A full list of abbreviations used in this article is provided in Supplementary Table S1.

Based on these tissue-segmented MDTs, we constructed a Common Hierarchical Parcellation to define homologous cortical and subcortical boundaries across species. The framework organizes brain regions into two additional levels: Level 1 macro-regions, which comprise nine major cortical and subcortical divisions, and Level 2 subdivisions, which represent finer-scale anatomical parcels defined by consistent anatomical landmarks and literature-supported homologies. Together, these levels form the Common Gray Matter Atlas, harmonizing parcellations across phylogenetically distant species within a unified coordinate system.

Atlas validation was performed along two dimensions (Fig. 1, right). (1) Cross-atlas validation quantified Dice similarity between the common atlas and multiple species-specific atlases, providing a voxelwise measure of regional correspondence relative to existing parcellations. (2) Cross-scale containment validation evaluated the spatial nesting of finer atlas regions within broader common parcels, using containment scores and perturbation analyses to characterize the degree of alignment and boundary correspondence across scales.

2.2. Cross-Species Parcellation Hierarchy

Figure 2 illustrates the hierarchical parcellation sequence from Level 0 through Level 1 and 2 across the four species. Panels (a–d) depict Level 0 structural compartment segmentation, showing automated 3D U-Net classification of gray matter (GM), white matter (WM), deep gray matter (DGM), and cerebellum (CBL) in human, rhesus, marmoset, and mouse MDTs, respectively. This segmentation establishes the basic tissue architecture on which all higher-order divisions are defined.

From these structural compartments, the atlas extends to Level 1 macro-regions, representing nine major divisions—frontal (FRO), parietal (PAR), temporal (TEM), occipital (OCC), insular (INS), olfactory (OLF), cingulate (CIN), basal ganglia (BG), and thalamic (THL) systems. These macro-regions, shown across species in Figure 2 (e–h), are defined by consistent anatomical landmarks and human-centric reference mapping while accommodating species-specific anatomical variation.

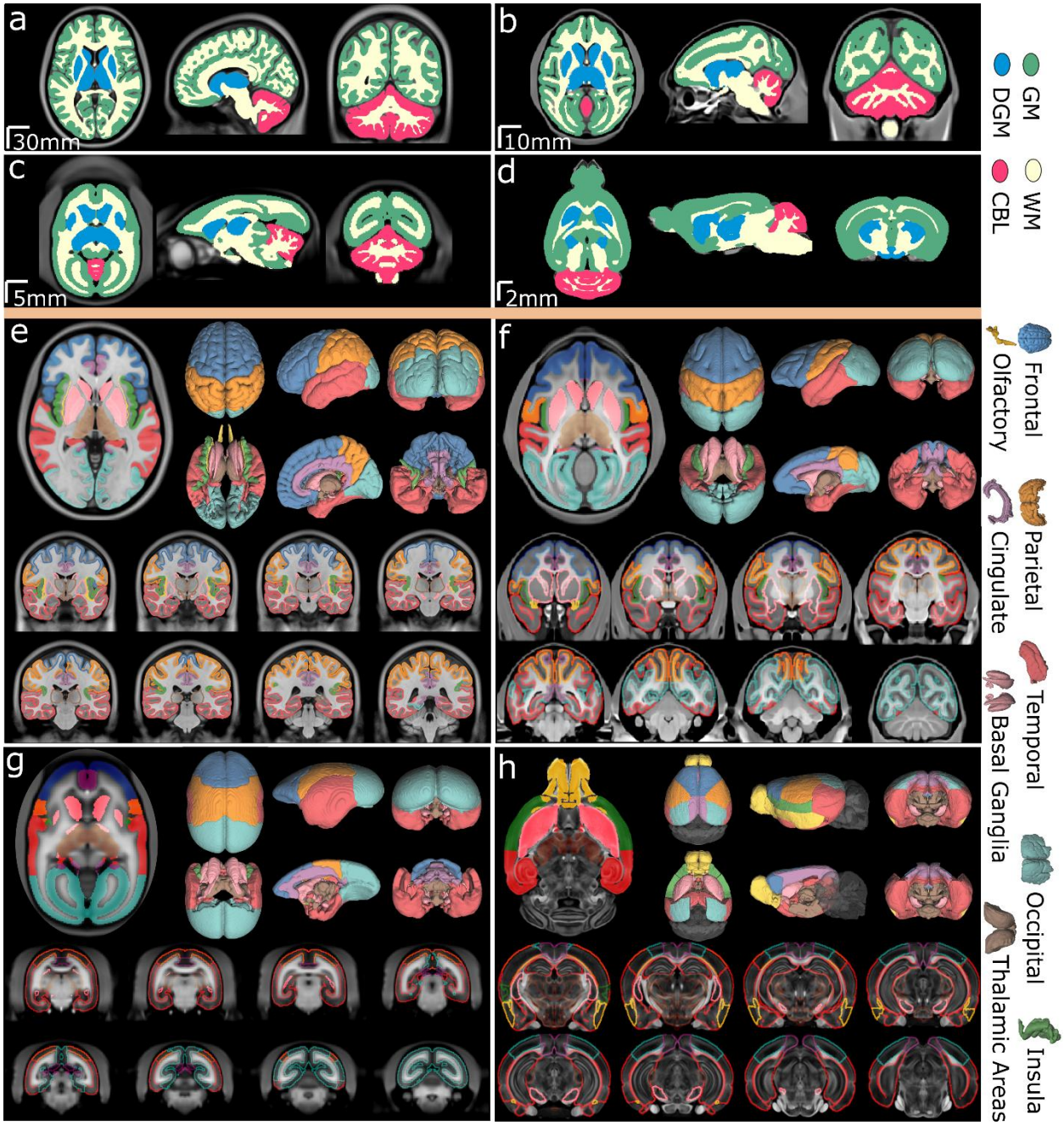

Figure 2 | Cross-species construction of the common anatomical atlas. (a–d) Tissue segmentation (structural compartments) for human **(a)**, rhesus macaque **(b)**, marmoset **(c)**, and mouse **(d)**. High-resolution T1- and T2-weighted MRI scans were processed using U-NET Studio for automated segmentation into five classes: gray matter (GM, green), white matter (WM, yellow), deep gray matter (DGM, blue), cerebellum (CBL, pink), and cerebrospinal fluid (not shown). Representative sagittal, coronal, and axial views illustrate the structural compartments in each species. **(e–h)** Lobe-level gray matter parcellation (Level-1) for human **(e)**, rhesus **(f)**, marmoset **(g)**, and mouse **(h)**. Nine macro-regions—frontal, parietal, temporal, occipital, insula, cingulate, basal ganglia, thalamus, and olfactory—were defined using consistent anatomical landmarks and human-centric mapping. Cortical regions are displayed with

harmonized color-coded boundaries and abbreviations, providing the scaffold for Level-2 subdivisions developed in subsequent analyses. Full mosaic views for all species are given in supplementary figures S1 through S4.

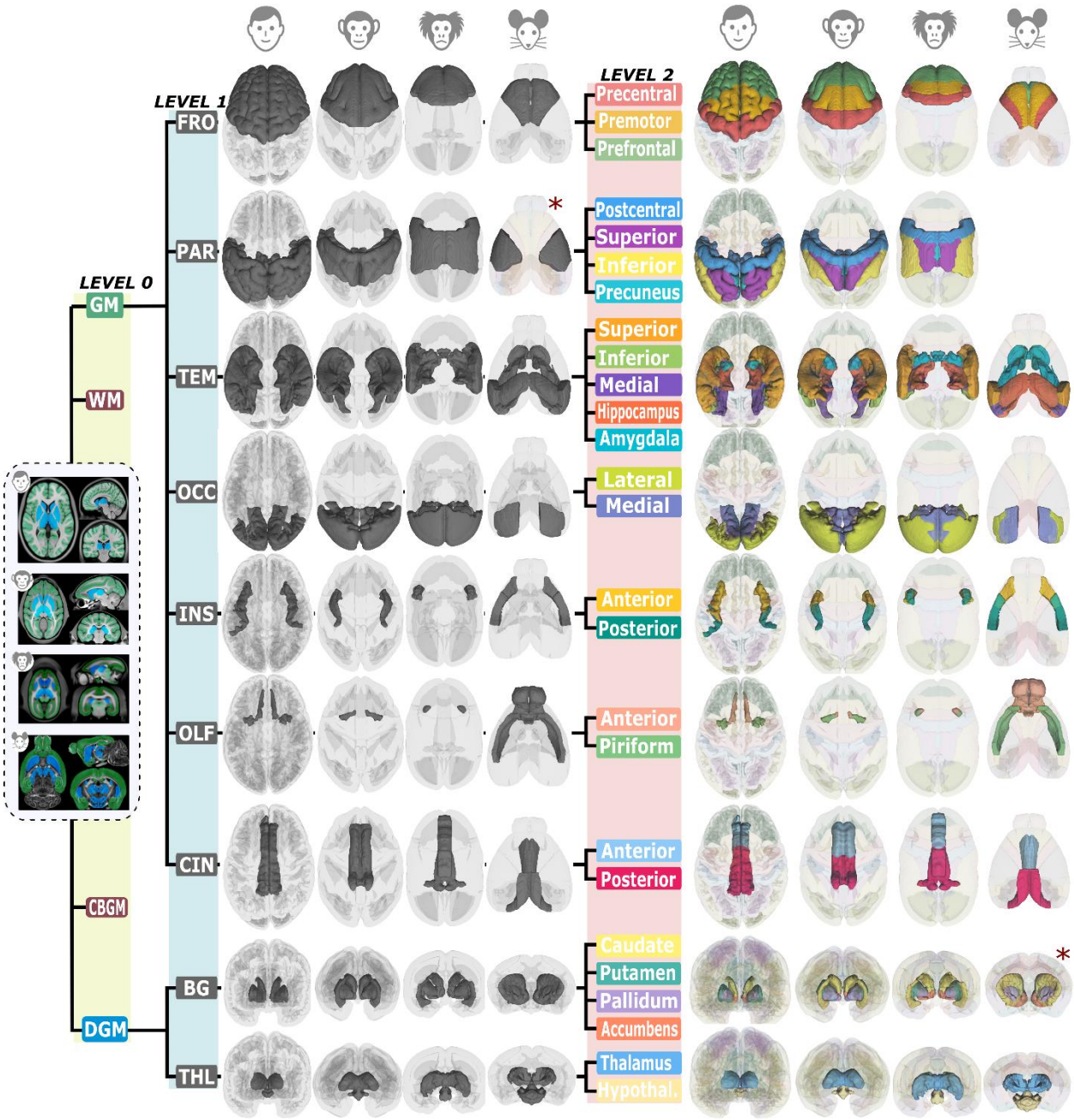

Figure 3 | Cross-species parcellation hierarchy. The hierarchical relationships between grey matter parcels are shown across four species (human, rhesus, marmoset, mouse). Four tissue compartments form level-0 of the hierarchy: Grey Matter (GM), White Matter (WM), Cerebellar Grey Matter (CBGM), and Deep Grey Matter (DGM). The GM and DGM compartments form root structures for a total of nine level-1 structures across species (grey). These level-1 structures are further subdivided into a total of 26 level-2 structures in primates and 21 level-2 structures in rodents. Level-1 PAR and level-2 Caudoputamen

structures are undivided in rodents (denoted by *). Parcel colors are harmonized across species to facilitate direct visual comparison.

Figure 3 expands the view to show the full hierarchical organization of Level 1 and 2 structures. GM and DGM compartments form the root of the hierarchy, branching into nine Level 1 divisions and a total of 26 Level 2 subdivisions in primates and 21 in rodents. Harmonized color schemes enable direct cross-species comparison. The parietal (PAR) lobe and the caudoputamen remain undivided in rodents (denoted by *), reflecting both true anatomical differences and segmentation limitations. This hierarchical framework unifies cortical and subcortical gray matter organization, establishing a scalable anatomical reference for comparative and network-level analyses.

2.3. Volumetric Composition Across Species

Figure 4 quantifies species differences in volumetric organization across Level 2 regions. Panel (a) presents dumbbell plots of normalized Level 2 volume fractions within each species. Volumetric fractions revealed clear species differences across cortical and subcortical regions (Fig. 4a, b). Humans showed the largest proportional volumes in prefrontal (0.22) and parietal (0.19) cortex, consistent with well-established expansion of association cortices in primates and especially in humans[13–15]. Rhesus macaques also showed elevated prefrontal (0.15) and superior temporal (0.16) fractions, in agreement with comparative MRI and anatomical studies highlighting enlarged association and temporal systems in Old World primates[16,17].

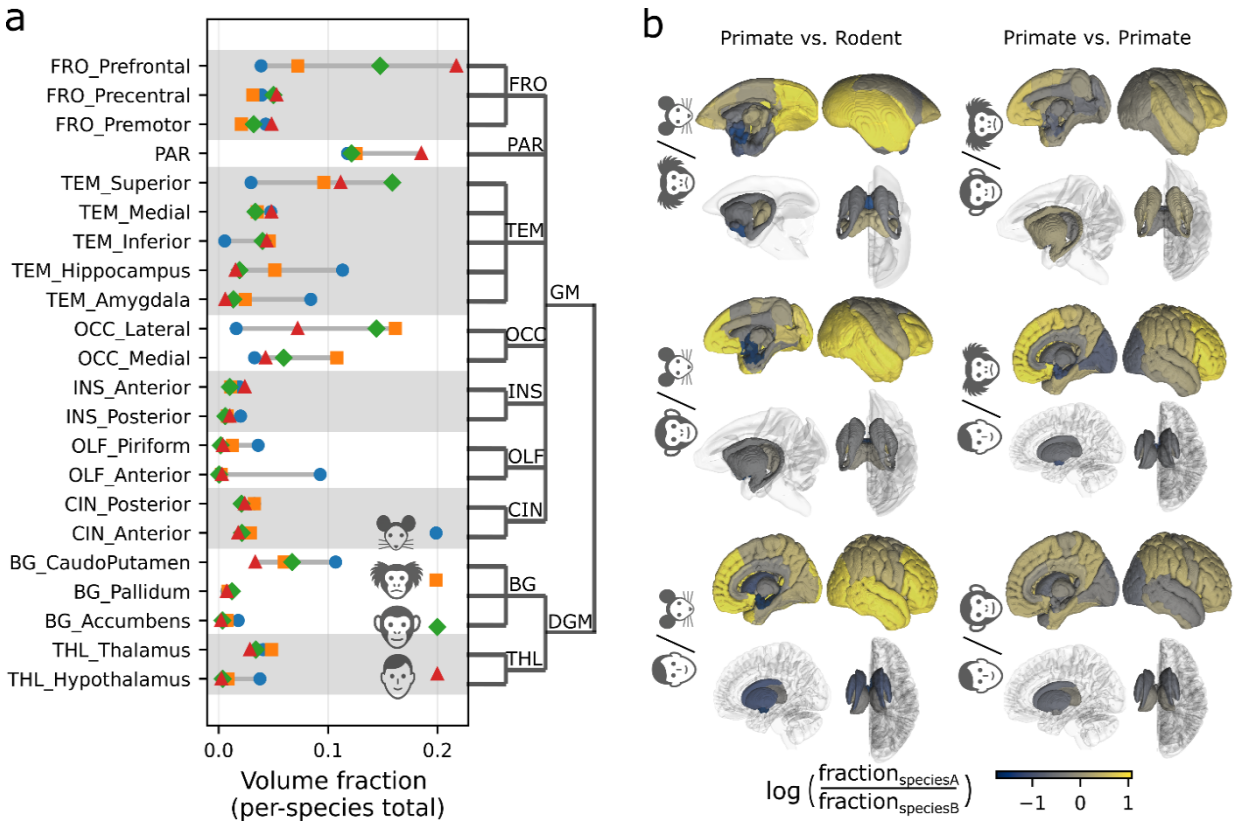

Figure 4 | Volumetric composition. **(a)** Dumbbell plot of Level-2 volume fractions (each species normalized to its own total). For each region, colored markers denote species values. **(b)** Pairwise 3D

maps of relative volumetric investment for six interspecies comparisons. Colors encode $\log(fraction_{species\ A}/fraction_{species\ B})$; positive values indicate greater fractional investment in species A. For each comparison, color is mapped onto the species A brain template.

Marmosets exhibited comparatively higher fractions in lateral and medial occipital cortex (0.16 and 0.11), as well as appreciable superior temporal volume (0.10), consistent with their relatively extensive visual and multisensory cortical territories[18,19]. In contrast, mouse showed the highest proportional volumes in hippocampus (0.11), amygdala (0.08), anterior olfactory regions (0.09), and piriform cortex (0.036), matching the prominence of allocortical and olfactory systems described in rodents[20,21]. Across species, deep gray-matter regions, including pallidum, accumbens, and thalamus, varied more modestly in fractional volume than the cortical systems, in line with general principles of coordinated but constrained scaling across brain structures described in comparative mammalian neuroanatomy[22,23]. Panel (b) displays pairwise 3D maps of relative volumetric investment, color-coded by the logarithmic ratio of fractional volumes between species. These maps reveal cortical expansion in humans and stronger limbic weighting in rodents, reflecting both conserved and lineage-specific scaling principles. Together, these results indicate that the common atlas enables comparison of homologous regional definitions and highlights volumetric allocation differences that distinguish primate associative enlargement from rodent limbic specialization.

2.4. Validation of the Common Atlas

We evaluated the anatomical fidelity of the common atlas at multiple scales: (i) cross-atlas validation within humans, (ii) correspondence with the Allen Brain Atlas (ABA, major) in mouse, and (iii) containment validation against finer scale species-specific atlases.

2.4.1. Validation of the Common Human Atlas Using Cross-Atlas Dice Similarity

The common human atlas showed broadly consistent alignment with standardized Neuroparc[4] parcellations. Most Level-2 regions matched 4–8 labels across reference atlases (e.g., hippocampus: 8; precuneus: 6; nucleus accumbens: 2). Regions such as the hypothalamus and finer olfactory subdivisions were not consistently labeled or directly mappable. However, all Level-2 parcels were evaluated where correspondence could be established.

Violin plots of Dice similarity demonstrated that Common vs. Others typically achieved higher overlap than Others vs. Others, indicating greater internal consistency of the common atlas relative to inter-atlas variability (Fig. 5a). Scatterplots of ΔMedian Dice versus absolute Dice confirmed that nearly all regions fell above zero, showing that the common atlas provided superior, or at least equivalent, anatomical overlap. Cortical regions displayed greater variability, whereas subcortical structures such as the thalamus and putamen were more stable, consistent with prior benchmarks reporting poor cortical but stronger subcortical concordance across human atlases[1–4].

Certain cortical regions, such as the superior parietal lobule (SPL), showed lower correspondence (median Dice ≈ 0.37), although the common atlas still performed slightly better than inter-atlas comparisons. The expanded Dice matrix (Fig. 5b) confirmed low similarity across all atlases, highlighting the variability of SPL boundaries in existing human parcellations. However, overlaying

the common SPL on T1w MRI demonstrated clear alignment with the superior parietal gyrus, supporting the anatomical validity of the common definition despite poor cross-atlas agreement.

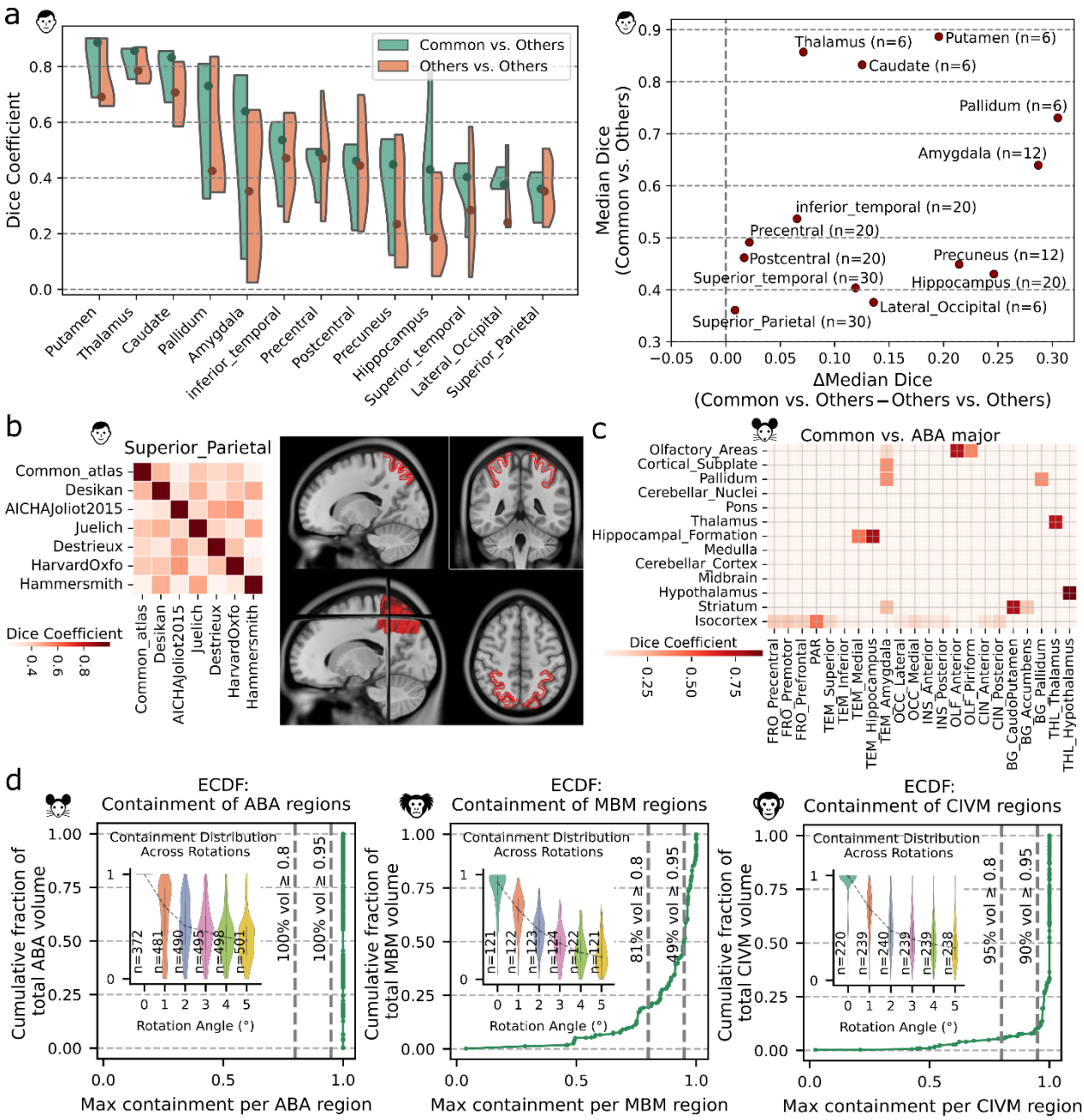

Figure 5 | Validation of the common cross-species framework. (a) Validation of human parcellation using cross-atlas Dice similarity. Dice coefficients were computed for each common atlas region against Neuroparc references[4] and compared to overlaps among non-common atlases. Violin plots show region-wise distributions; scatterplots summarize median Dice and ΔMedian differences. Most regions demonstrated stronger overlap with the common atlas than with each other. **(b)** Expanded analysis of superior parietal lobule, the weakest Dice performer in panel a. Left: Dice matrix comparing the common SPL to six Neuroparc atlases. Right: common SPL overlaid on T1w MRI, showing alignment with gyral boundaries despite low inter-atlas concordance. **(c)** Dice similarity between the 13 major divisions of the Allen Brain Atlas (ABA) and

common Level-2 regions. High Dice values occurred where there was direct correspondence (e.g., thalamus, hypothalamus, olfactory, hippocampus). Broad ABA parcels such as isocortex showed low Dice because they were subdivided into multiple human-centric parcels. **(d)** Cross-species finer-scale containment validation. Mouse regions (ABA) showed perfect containment (score = 1.0). Rhesus (CIVM) exhibited high correspondence, with 95% of volume achieving containment ≥0.80 and 90% ≥0.95. Marmoset (MBM) showed 81% of volume achieving ≥0.80 and 49% ≥0.95. Differences partly reflect atlas resolution (121 regions in MBM vs. 220 in CIVM and 372 in ABA). Lower-containment cases reflect reliance on secondary atlases where homology was not clearly defined. Insets illustrate the decay of containment scores under perturbational rotation, confirming the sensitivity of the metric to spatial disruption.

2.4.2. Validation Against Mouse ABA Major Regions

Dice similarity analyses revealed two complementary patterns. For ABA regions with direct correspondence to common parcels, such as hypothalamus, thalamus, olfactory areas, and hippocampus, Dice values were high, reflecting strong spatial alignment (Fig. 5c). In contrast, broad ABA categories like *Isocortex* showed lower values because these regions were intentionally subdivided across multiple common ROIs to match human-centric definitions. This outcome indicates that the common framework preserves homologous subcortical structures with high fidelity, while deliberately enforcing finer cortical subdivisions to support cross-species consistency.

2.4.3. Containment Validation Against Finer-Scale Species-Specific Atlases

Containment validation was used to benchmark anatomical correspondence between finer-scale species-specific atlases and the common framework (Fig. 5d). The containment metric measures the fraction of each finer ROI that is fully contained within its corresponding common parcel, thereby quantifying how well the broader common regions align with and respect the boundaries of more detailed species-specific parcellations. This provides a direct test of whether the common atlas captures homologous anatomical divisions without overstepping finer boundaries.

Fig. 5d insets illustrate the effect of spatial perturbation: containment scores declined systematically with increasing rotation, reflecting degraded anatomical alignment between finer atlas regions and common parcels. At the same time, the number of participating ROIs increased under rotation, for example, from 372 at 0° to 501 at 5° in the ABA, because spatial misalignment allowed additional regions to form weak matches with non-dominant common labels. This pattern stems from the max-retention strategy: finer ROIs that previously showed zero overlap could re-enter the distribution once even minimal overlap with a rotated common label was established. Annotated violin plots captured this dual effect, showing (1) a larger pool of ROIs included under rotation, and (2) systematically lower containment scores, particularly in the upper quantiles. Together, these results demonstrate the sensitivity of the containment metric to spatial perturbation and validate its utility as a benchmark of anatomical alignment.

Across species, validation confirmed strong correspondence between common parcels and species-specific atlases. In mouse, where parcellation was directly anchored to the Allen Brain Atlas (ABA), all regions exhibited perfect containment (score = 1.0). In rhesus, compared with the CIVM atlas, 95% of volume achieved a containment score ≥0.80 and 90% ≥0.95, demonstrating high fidelity to established boundaries. In marmoset, compared with the MBM atlas, 81% of volume achieved ≥0.80 and 49% ≥0.95. These differences partly reflect atlas resolution: the MBM

includes only 121 regions, compared to 220 in CIVM and 372 in ABA, and a smaller number of parcels is expected to yield lower containment scores.

The minority of regions with low containment reflect deliberate design choices. Where a primary atlas (e.g., MBM) did not provide clear homology, secondary resources (e.g., Paxinos, Brain/MINDS) were used to reach cross-species consistency. Given the well-documented inconsistencies among published atlases, occasional low containments are expected and reflect our emphasis on preserving biologically plausible, literature-supported homologies rather than enforcing strict one-to-one correspondence with any single atlas.

3. Discussion:

In this study, we introduce a standardized anatomical framework that aligns cortical and subcortical parcellations across rodents, nonhuman primates, and humans. A central achievement was the construction of population-averaged minimal deformation templates (MDTs) for each species, which provide anatomically consistent reference spaces for cross-species alignment. While humans and marmosets already had established MDTs (ICBM2009a and Brain/MINDS, respectively), we generated new MDTs for mouse, rat, and rhesus macaque using high-resolution MRI and iterative diffeomorphic averaging. To further ensure consistency across species, we applied a 3D U-Net segmentation network to classify tissue compartments into gray matter, white matter, deep nuclei, cerebellum, and CSF in a uniform manner. Building on these MDTs and tissue segmentations, we delineated a common hierarchical atlas that enables direct comparison of cortical and subcortical organization across species within a unified coordinate system.

Our analyses also revealed systematic differences in the volumetric ratios of major brain regions across species, providing quantitative insights into conserved versus lineage-specific organizational features. Humans showed disproportionately larger allocations to the frontal and parietal cortices, consistent with expanded associative functions, whereas rhesus macaques exhibited a relatively greater investment in temporal regions. Rodents, in contrast, devoted proportionally more volume to limbic and sensorimotor structures such as the hippocampus, amygdala, olfactory regions, and caudoputamen. Despite these divergences, several subcortical and paralimbic structures, including the thalamus, pallidum, accumbens, and insula, demonstrated relatively conserved volumetric scaling across species. These findings highlight how a common atlas grounded in MDTs and consistent segmentation can expose cross-species patterns of cortical expansion and subcortical conservation, offering a framework to advance translational neuroscience.

Many existing atlases have been developed independently within single species and use heterogeneous template-construction methods, making it difficult to achieve consistent anatomical definitions across resources. Although population-based templates such as ICBM2009a exist for humans[9], comparable MDT-style population templates are less widely available in nonhuman species. In addition, several cross-species and primate atlases have focused primarily on cortical surfaces or macro-architectural cortical divisions, with comparatively less standardized coverage of subcortical and deep gray structures essential for whole-brain analyses[5,7]. These differences in template construction and anatomical coverage contribute to the

difficulty of establishing fully consistent whole-brain parcellations across species. By establishing MDTs across multiple species and harmonizing them into a single atlas framework, our study addresses these limitations and provides population-based cross-species reference system applicable across rodents, nonhuman primates, and humans.

Another noteworthy contribution of this study is the adoption of a 3D U-Net–based tissue segmentation framework as the foundation for Level-0 parcellation. Our approach applied a unified deep-learning model to classify gray matter, white matter, deep nuclei, cerebellum, and cerebrospinal fluid across all species. This strategy reduces variability introduced by manual delineation or heterogeneous processing methods and ensures that higher-level parcellations are grounded in a consistent tissue definition. By standardizing this first step of anatomical labeling, the 3D U-Net segmentation provides a robust and reproducible baseline for cross-species comparisons, complementing the use of population-averaged MDTs as common spatial anchors.

Nevertheless, several limitations of the current work must be acknowledged. Some structures—including the claustrum, substantia nigra, and subthalamic nucleus—were excluded because reliable segmentation was not feasible across MRI datasets for all species. The claustrum forms a thin, sheet-like structure between the insula and putamen, and both the substantia nigra and subthalamic nucleus are small deep nuclei with low intrinsic MRI contrast; even in humans, robust segmentation typically requires ultra–high-resolution or specialized contrast and extensive manual delineation[24–26]. Consequently, many widely used MRI-based atlases omit these nuclei or include them only when high-resolution data are available for a particular species. In the striatum, caudate–putamen separation proved difficult to identify in mouse MRI, requiring consolidation into a single caudoputamen parcel due to the absence of a clear anatomical boundary; the Allen Mouse Brain Atlas likewise treats caudoputamen (CP) as a single complex in its reference annotation[27]. In contrast, rodents lack the definite sulcal and gyral segmentation that characterizes the primate parietal lobe; the mouse PAR parcel corresponds primarily to its continuous somatosensory territory, whereas primates possess a subdivided parietal cortex comprising postcentral, superior, inferior, and precuneus regions[28,29]. To preserve lobe-level comparability while acknowledging these anatomical differences, we retained a single undivided PAR parcel in mouse. These exclusions therefore reflect a combination of practical segmentation limitations and true absence of homology. Despite such gaps, the consistent parcellation achieved across retained regions may facilitate cross-species comparability relative to species-specific atlases, where definitions often diverge widely.

Looking ahead, the atlas can be refined to capture finer levels of granularity. A promising next step is the introduction of Level 3 subdivisions in systems with pronounced functional specialization, such as the hippocampus, thalamus, and amygdala. Higher-resolution parcellations in these domains will enable the direct comparison of questions related to intra-system organization, such as hippocampal subfields or thalamic nuclei specializations, across species. Such expansions will enhance the translational utility of the atlas, linking microcircuit-level distinctions to macroscale pathways and enabling more mechanistic models of brain organization.

In sum, the common atlas offers a broadly applicable resource for comparative and translational neuroscience. It delivers consistent parcellation across divergent species and enables principled integration of diverse modalities.

4. Online Methods

4.1. Construction of Minimal Deformation Templates

To ensure anatomically consistent cross-species alignment, we constructed species-specific minimal deformation templates (MDTs). Except for humans (standard template), each MDT was generated separately, aligned to the AC–PC axis, and rigidly positioned with the origin at the anterior commissure (AC). This procedure follows the general principles of population-based template building implemented in ANTs, where iterative symmetric diffeomorphic registration is used to construct an unbiased minimal-deformation group average[11,12]. All atlas labels and analyses refer to these MDT spaces.

4.1.1. Mouse MDT

All mouse procedures were approved by the Duke Institutional Animal Care and Use Committee (Duke IACUC approval A169-20-08). Male C57BL/6J mice were obtained from Jackson Laboratories and actively stained using a protocol involving transcardial infusion of ProHance in 10% buffered formalin, followed by post-fixation and equilibration[30,31].This reduces T1 to ~100 ms, enabling shorter TR and improved signal-to-noise ratio.

Imaging was performed on a 9.4 T vertical Oxford magnet with Resonance Research gradients (BFG 88/41) using a 13 × 25 mm solenoid coil tuned to 300 MHz. A Stejskal–Tanner sequence with compressed sensing achieved 25 µm isotropic resolution. We acquired 61 diffusion-weighted volumes (b = 3000 s/mm²) and 6 baselines (TR = 80 ms, TE = 14 ms) with uniformly distributed gradient directions. Compressed sensing[32,33] (BART[34]) at 8× acceleration reduced the total acquisition time to ~19 h per 4D dataset.

After acquisition, DWIs were corrected for eddy currents by registering each diffusion-weighted volume to the averaged baseline. Denoising used a local spatiotemporal noise model across k- and q-space[30]. Datasets were then reconstructed in DSI Studio using GQI.

The mouse MDT was constructed from 22 specimens (17 at 25 µm; 5 originally at 15 µm and downsampled to 25 µm). After preprocessing and coarse spatial checks, an initial template was formed via pairwise affine registrations: for each specimen, the set of affines to all others was averaged to obtain a median-space transform. Applying these transforms produced the initial mean. We then ran six iterative register-to-template cycles: (i) diffeomorphic registration to the current MDT, (ii) warping and averaging, (iii) averaging all deformation fields to visualize variability, and (iv) warp-dependent blurring proportional to mean deformation magnitude to focus updates on high-variance loci. This yielded a minimal-deformation population mean.

Labels in MDT space were generated by registering the final MDT to a symmetric mouse atlas and inverting the transforms. The final template was cropped and rigidly adjusted so the origin was at AC and AC/PC lay on a common axial slice.

4.1.2. Rat MDT

Rat brain MRI were acquired at the Duke Center for In Vivo Microscopy (CIVM) under IACUC approval. Animals were actively stained using the same protocol as mice[30,31]. For rats, mandibles were removed to allow use of a smaller RF coil and improve sensitivity at high spatial resolution.

Specimens were scanned on a Bruker 7 T Avance III with high-performance gradients (Resonance Research, BFG 102/60; 1000 mT/m). Acquisition used a Stejskal–Tanner spin-echo sequence (TR = 100 ms, TE = 22.5 ms, b = 3000 s/mm²) with 61 diffusion directions uniformly distributed on the sphere; a b0 image was acquired after every 10th diffusion-weighted scan. Data were streamed to an HPC cluster and reconstructed with compressed sensing[32,33]. Baselines were averaged; all DWIs were then registered to the baseline with ANTs[30,35].

A rat MDT was constructed from 18 Wistar rats (~P90) using the SAMBA pipeline[36], built on ANTs. Registration was based on DWI contrast. To obtain symmetric labels, the final MDT was registered to the symmetric Wistar rat atlas, and inverse transforms were applied to warp the label set into MDT space. The final MDT was cropped and rigidly adjusted so the origin was at AC and AC/PC lay on a common axial slice.

4.1.3. Marmoset MDT

MRI data were obtained from the Brain/MINDS Marmoset Brain MRI dataset[37]. Marmoset atlas data were derived from Marmoset Brain Mapping (MBM) v3[10]. We applied minimal spatial header adjustments to achieve AC-centered coordinates. Specifically, the NIfTI srow matrix was modified to (units in mm):

0.2 0 0 -14.6

0 0.2 0 -25.7

0 0 0.2 -13.3

These changes preserve MBM v3 image content while placing the AC at (0,0,0) and maintaining isotropic 0.2 mm voxels. Subsequent rigid checks ensured AC–PC alignment.

4.1.4. Rhesus Macaque MDT

Rhesus macaque T1-weighted images were derived from The PRIMatE Data Exchange (PRIME-DE) via International Neuroimaging Data-sharing Initiative (INDI)[38]. Each volume was rigidly aligned to AC–PC, with the origin set at AC. We constructed a minimal deformation template (MDT) using an iterative diffeomorphic averaging procedure implemented in ANTs[12]. The final template was recentered at the anterior commissure (AC) and resampled to isotropic resolution to facilitate label transfer.

4.1.5. Human MDT

For humans, we adopted the widely used ICBM152 Nonlinear Asymmetrical 2009a template (ICBM2009a)[9] as the species reference space. This template is a population-average of 152 adult (age 18-44y) T1-weighted MRI volumes, generated using iterative nonlinear registration to minimize anatomical variability across individuals. The final template was AC–PC aligned, with the origin set at the anterior commissure (AC), and provides an established standard for human neuroimaging studies.

4.2. Construction of Brain parcellations

This work describes a two-level hierarchy to define common regions of interest across species. Level-1 parcellation comprised nine cortical and subcortical divisions, delineated using major anatomical boundaries such as cortical lobes and clearly identifiable deep structures in high-resolution MRI. Level-2 further subdivided Level-1 regions along secondary anatomical margins such as cortical gyri, sulci, or known cytoarchitectonic transitions. Subdivisions were primarily established in humans using high-resolution MRI and aligned with anatomical conventions from widely used atlases. Homologous regions in animals were then identified using a literature-guided approach, incorporating prior anatomical and histological studies, species-specific atlases, and patterns of regional naming and usage in the comparative neuroimaging literature. Structural compartment segmentation was performed in U-NET Studio[39] to generate probability maps for gray matter, white matter, deep nuclei, cerebellum, and CSF from high-resolution MRI. The common parcellation framework was subsequently generated in DSI Studio[40].

Because cross-species homology is not always uniquely defined, particularly in higher-order association areas, the framework prioritized three principles: (i) preserve regional definitions widely used in existing atlases, (ii) maximize cross-species consistency where boundaries could be reasonably identified in MRI, and (iii) retain functional interpretability. In some cases, functional considerations were decisive. For example, the superior temporal parcel combines the superior and middle temporal gyri in humans, which cannot be reliably separated in nonhuman primates or rodents but together form a coherent auditory–language system. By contrast, the superior, middle, and inferior frontal gyri, though clearly identifiable in humans, were not retained as separate parcels due to the absence of clear homologues in lower species. Instead, functionally grounded regions such as precentral, premotor, and postcentral were emphasized to preserve sensorimotor comparability. Similarly, olfactory parcels were included despite their small size in humans, reflecting their critical role in rodent and marmoset cognition and a rich comparative literature. The medial temporal parcel in mouse encompasses the rhinal complex (entorhinal, perirhinal, postrhinal), while in primates it includes the entorhinal and parahippocampal cortices; across species, this region mediates hippocampal–neocortical interactions. Conversely, structures such as the claustrum, substantia nigra, and subthalamus, while homologous in principle, were excluded due to segmentation challenges in cross-species MRI datasets.

Primary species (human, rhesus macaque, marmoset, and mouse) were delineated directly from MRI-based parcellations. To extend coverage, rat parcellations were derived by warping the mouse atlas, using MRI-based alignment. These warped parcellations provided approximate coverage for additional species while preserving consistency with the core cross-species framework.

For each Level-2 region, homologues were identified from one or more standard atlases: FreeSurferSeg (human)[41,42], Brodmann (human)[43], the Allen Brain Atlas (mouse)[27], CIVM rhesus atlas (rhesus macaque)[44], Inia19–NeuroMaps (rhesus macaque)[45], Brain/MINDS (marmoset)[46], MBM atlas (marmoset)[47], and Paxinos (marmoset)[48], with priority given to sources providing the clearest anatomical or functional correspondence. Where multiple atlases were necessary (e.g., in marmoset and rhesus), boundaries were cross-validated across references. Detailed listings of

atlas sources, supporting references, and region coverage for each Level-2 parcel are provided in Table 1.

Table – 1. Atlas sources and regional definitions in the common framework.

Common region (short label)	Atlas sources	Region coverage
FRO_Precentral (PreC)	**H:** BA, FSS; **Rh:** CIVM; **Mz:** Paxinos, MBM, BMA; **Mo:** ABA	Primary motor cortex across species.
FRO_Premotor (PreM)	**H:** BA, FSS; **Rh:** CIVM; **Mz:** Paxinos, MBM, BMA; **Mo:** ABA	Secondary motor areas retained for cross-species functional consistency.
FRO_Prefrontal (PreF)	**H:** BA, FSS; **Rh:** CIVM; **Mz:** MBM, Paxinos, BMA; **Mo:** ABA	**Primates:** includes dorsolateral, ventrolateral, medial prefrontal, and orbitofrontal areas. **Mouse:** encompasses prelimbic, infralimbic, and orbital regions.
PAR (Parietal)	**H:** FSS; **Rh:** CIVM; **Mz:** Paxinos, MBM, BMA; **Mo:** ABA	**Primates:** postcentral, superior, inferior, and precuneus divisions. **Mouse:** undivided (somatosensory areas)
TEM_Superior (TemS)	**H:** FSS; **Rh:** INM; **Mz:** Paxinos, MBM, BMA; **Mo:** ABA	Human includes superior and middle temporal gyri; auditory association areas across all species; language/auditory functions emphasized.
TEM_Inferior (TemI)	**H:** FSS; **Rh:** INM; **Mz:** MBM, BMA; **Mo:** ABA	**Primates:** inferior temporal (IT) areas. **Mouse:** approximated by ectorhinal (ECT) (ventral adjacency to auditory cortex; lateral adjacency to medial temporal areas. ECT lacks the laminar complexity and cortical expansion seen in primate IT, yet its connectivity and functional responses suggest a comparable role in integrating visual and memory-related cues. It receives input from ventral stream visual areas and shows activation patterns sensitive to motion, object size, and stimulus familiarity[49,50]. These properties align with IT's role in object-level discrimination and multimodal convergence. While not a strict anatomical

		homologue, ECT is close functional analog to primate IT).
TEM_Medial (TemM)	**H:** FSS; **Rh:** INM; **Mz:** Paxinos, MBM, BMA; **Mo:** ABA	**All species:** rhinal/parahippocampal complex, including entorhinal, perirhinal, postrhinal (mouse) / parahippocampal (primates); supports hippocampal–neocortical interactions[51,52].
TEM_Hippocampus (Hipp)	**H:** FSS; **Rh:** CIVM; **Mz:** MBM, BMA; **Mo:** ABA	Conserved structure across species.
TEM_Amygdala (Amyg)	**H:** FSS; **Rh:** CIVM; **Mz:** Paxinos, MBM, BMA; **Mo:** ABA	Preserved across species; limbic/olfactory interfaces[20].
OCC_Lateral (OccL)	**H:** FSS; **Rh:** INM; **Mz:** MBM, BMA, Paxinos; **Mo:** ABA	**Human/Rhesus:** superior, middle, inferior occipital gyri. **Marmoset:** includes V1a, V2v, V3v, V2L, V3L. **Mouse:** lateral visual areas grouped.
OCC_Medial (OccM)	**H:** FSS; **Rh:** INM; **Mz:** MBM, BMA, Paxinos; **Mo:** ABA	**Human/Rhesus:** lingual, cuneus, calcarine. **Marmoset:** includes V1b, V2M, A19M. **Mouse:** medial visual areas grouped.
INS_Anterior (InsA)	**H:** FSS; **Rh:** CIVM; **Mz:** Paxinos, MBM, BMA; **Mo:** ABA	Agranular insula with adjacency to piriform emphasized[53].
INS_Posterior (InsP)	**H:** FSS; **Rh:** CIVM; **Mz:** Paxinos, MBM, BMA; **Mo:** ABA	Granular insula; consistent across primates.
CIN_Anterior (CingA)	**H:** BA, FSS; **Rh:** CIVM; **Mz:** Paxinos, MBM, BMA; **Mo:** ABA	Anterior vs posterior split supported by cytoarchitecture/connectivity[54].
CIN_Posterior (CingP)	**H:** BA, FSS; **Rh:** CIVM; **Mz:** Paxinos, MBM, BMA; **Mo:** ABA	Matches posterior cingulate/retrosplenial homologues[54].
OLF_Anterior (OlfA)	**H:** FSS; **Rh:** CIVM; **Mz:** Paxinos, MBM, BMA; **Mo:** ABA	AnteroMedial adjacency to Piriform in all species; routes olfactory inputs to Piriform[55]; Olfactory bulb included in human and mouse.

OLF_Piriform (Pir)	**H:** FSS; **Rh:** CIVM; **Mz:** Paxinos, MBM, BMA; **Mo:** ABA	Piriform preserved separately; adjacency to insula[53]
BG_CaudoPutamen (CPu)	**H:** FSS; **Rh:** CIVM; **Mz:** MBM, BMA, Paxinos; **Mo:** ABA	Core striatal component[56]; subdivided into caudate + putamen in primates; undivided in rodents due to segmentation difficulties.
BG_Accumbens (NAc)	**H:** FSS; **Rh:** CIVM; **Mz:** MBM, BMA, Paxinos; **Mo:** ABA	Kept distinct for translational relevance[56].
BG_Pallidum (Pal)	**H:** FSS; **Rh:** CIVM; **Mz:** MBM, BMA; **Mo:** ABA	Globus pallidus included[56]; robust segmentation across species.
THL_Thalamus (Thal)	**H:** FSS; **Rh:** CIVM; **Mz:** MBM, BMA; **Mo:** ABA	Well-defined across species; treated separately from basal ganglia.
THL_Hypothalamus (Hypo)	**H:** FSS; **Rh:** CIVM; **Mz:** MBM, BMA; **Mo:** ABA	Well-defined across species.
Excluded (Claustrum, Substantia Nigra, SubThalamicNuclei)	—	Homologous in principle but excluded due to MRI segmentation limitations.

Abbreviations (atlas sources)

BA = Brodmann areas[43] (human)

FSS = FreeSurferSeg[41,42] (human)

ABA = Allen Brain Atlas[27] (mouse)

CIVM = Center for In Vivo Microscopy atlas[44] (rhesus)

INM = Inia19–NeuroMaps[45] (rhesus)

MBM = Marmoset Brain Mapping atlas[47]

BMA = Brain/MINDS Marmoset Reference Atlas[46]

Paxinos = Paxinos histological atlas[48] (marmoset)

4.3. Validation of the Common Atlas Across Scales and Species

4.3.1. Validation of Human Parcellation Using Neuroparc Atlases

To evaluate the anatomical consistency of the common human atlas, we compared each Level-2 region against corresponding regions from standardized human parcellations in the Neuroparc repository[4]. Candidate matches were identified by flexible text-string matching of region labels and cross-checked against anatomical conventions. Binary masks were constructed for each atlas, and Dice similarity coefficients were computed to quantify voxel-level overlap. For each common region, Dice distributions were summarized as “Common vs. Others” (overlaps between the common atlas and each other atlas) and “Others vs. Others” (overlaps among non-common atlases). Region-level summary metrics included the median Dice similarity for “Common vs. Others” and the difference between “Common vs. Others” and “Others vs. Others” (ΔMedian). Dice validation excluded Neuroparc atlases with poor performance for each region, defined as an average Dice overlap <0.1 across other Neuroparc atlases.

4.3.2. Validation Against Mouse Allen Brain Atlas Major Regions

To evaluate correspondence between the common mouse parcellation and its source atlas, we compared Level-2 regions against the 13 major regions of the Allen Brain Atlas (ABA). Dice similarity coefficients were computed between each ABA major parcel and the set of common ROIs.

4.3.3. Containment Validation Using Finer-Scale Species-Specific Atlases

Containment scores were used to test whether the coarser common atlas respected the boundaries of finer-scale species-specific parcellations. For each finer ROI, we computed the voxel wise fractional overlap with all common regions and retained only the maximum containment score, ensuring that each ROI was matched to its best-fitting common label while ignoring partial overlaps with non-dominant regions. ROIs with zero or undefined containment were excluded from downstream violin plot visualizations.

To test anatomical resilience under spatial perturbation, common labels were rigidly rotated about a central axis in fixed angular increments, without resampling or interpolation. Containment scores were recomputed for each rotated configuration using the same max-fraction rule, enabling direct comparison of distributional shifts across angles. Validation was performed for mouse against the ABA, for rhesus against the CIVM atlas, and for marmoset against the MBM atlas. Containment distributions were summarized for each species to assess overall alignment.

Acknowledgments
Computational resources were provided by the Pittsburgh Supercomputing Center through NSF ACCESS allocations MED230052 and CIS200026.

Use of AI Tools
ChatGPT (OpenAI) was employed to aid in language refinement and to suggest initial code structures for figure visualizations. All analysis code was written exclusively by the authors, who take full responsibility for all scientific content, code implementation, and conclusions.

Author Contributions
Siva Venkadesh: Conceptualization, Methodology (Level-1/2 parcellations, cross-species homology definitions), Formal analysis, Software, Validation, Visualization, Writing – Original

Draft, Writing – Review & Editing, Supervision
Yuhe Tian: Software, Validation, Formal analysis, Visualization
Wen-Jieh Linn: Data Curation, Visualization
Jessica Barrios Martinez: Data Curation, Visualization, Writing – Review & Editing
Harrison Mansour: Data Curation, Resources, Writing – Review & Editing
David J. Schaeffer: Data Curation, Resources, Writing – Review & Editing
Diego Szczupak: Data Curation, Resources, Writing – Review & Editing
Afonso C. Silva: Methodology (marmoset), Resources, Writing – Review & Editing
G Allan Johnson: Conceptualization, Methodology (mouse, rat), Study oversight, Resources, Writing – Review & Editing, Funding acquisition.
Fang-Cheng Yeh: Conceptualization, Methodology (Level-0 tissue segmentation), Study oversight, Project administration, Resources, Writing – Review & Editing, Funding acquisition.

Funding
This work was supported by the National Institutes of Health grant R01NS120954. SV was supported in part by NIH grant R01MH134004.

Data Availability
The atlas data presented here are freely available at https://github.com/data-others/atlas for each species *(<species>_CHA.nii.gz)*

Code Availability
All analysis and figure-generation code supporting the findings of this study are archived at Zenodo (https://doi.org/10.5281/zenodo.17653309) in the directory *projects/common_cross_species_atlas/.*

.

REFERENCES

1. Arslan, S. *et al.* Human brain mapping: A systematic comparison of parcellation methods for the human cerebral cortex. *Neuroimage* 170, 5–30 (2018).
2. Klein, A. *et al.* Evaluation of 14 nonlinear deformation algorithms applied to human brain MRI registration. *Neuroimage* 46, 786–802 (2009).
3. Bohland, J. W., Bokil, H., Allen, C. B. & Mitra, P. P. The brain atlas concordance problem: quantitative comparison of anatomical parcellations. *PLoS One* 4, e7200 (2009).
4. Lawrence, R. M. *et al.* Standardizing human brain parcellations. *Sci Data* 8, 78 (2021).
5. Eickhoff, S. B., Yeo, B. T. T. & Genon, S. Imaging-based parcellations of the human brain. *Nat. Rev. Neurosci.* 19, 672–686 (2018).
6. Schaefer, A. *et al.* Local-global parcellation of the human cerebral cortex from intrinsic functional connectivity MRI. *Cereb. Cortex* 28, 3095–3114 (2018).
7. Donahue, C. J., Glasser, M. F., Preuss, T. M., Rilling, J. K. & Van Essen, D. C. Quantitative assessment of prefrontal cortex in humans relative to nonhuman primates. *Proc. Natl. Acad. Sci. U. S. A.* 115, E5183–E5192 (2018).
8. Wang, Y. *et al.* The Chimpanzee Brainnetome Atlas reveals distinct connectivity and gene expression profiles relative to humans. *Innovation (Camb.)* 6, 100755 (2025).
9. Fonov, V. S., Evans, A. C., McKinstry, R. C., Almli, C. R. & Collins, D. L. Unbiased nonlinear average age-appropriate brain templates from birth to adulthood. *Neuroimage* 47, S102 (2009).
10. Liu, C. *et al.* Marmoset Brain Mapping V3: Population multi-modal standard volumetric and surface-based templates. *Neuroimage* 226, 117620 (2021).
11. Avants, B. B. *et al.* The optimal template effect in hippocampus studies of diseased populations. *Neuroimage* 49, 2457–2466 (2010).
12. Avants, B. B. *et al.* A reproducible evaluation of ANTs similarity metric performance in brain image registration. *Neuroimage* 54, 2033–2044 (2011).
13. Kaas, J. H. The evolution of neocortex in primates. *Prog. Brain Res.* 195, 91–102 (2012).
14. Krubitzer, L. In search of a unifying theory of complex brain evolution. *Ann. N. Y. Acad. Sci.* 1156, 44–67 (2009).
15. Amunts, K. & Zilles, K. Architectonic mapping of the human brain beyond brodmann. *Neuron* 88, 1086–1107 (2015).
16. Rilling, J. K. & Insel, T. R. The primate neocortex in comparative perspective using magnetic resonance imaging. *J. Hum. Evol.* 37, 191–223 (1999).
17. Kaas, J. H. & Hackett, T. A. Subdivisions of auditory cortex and processing streams in primates. *Proc. Natl. Acad. Sci. U. S. A.* 97, 11793–11799 (2000).
18. Solomon, S. G. & Rosa, M. G. P. A simpler primate brain: the visual system of the marmoset monkey. *Front. Neural Circuits* 8, 96 (2014).
19. Paxinos, G., Watson, C., Petrides, M., Rosa, M. & Tokuno, H. The marmoset brain in stereotaxic coordinates. *Elsevier Academic Press* (2012).
20. Swanson, L. W. & Petrovich, G. D. What is the amygdala? *Trends Neurosci.* 21, 323–331 (1998).

21. Lledo, P.-M., Gheusi, G. & Vincent, J.-D. Information processing in the mammalian olfactory system. *Physiol. Rev.* 85, 281–317 (2005).
22. Aboitiz, F. & Montiel, J. F. From tetrapods to primates: conserved developmental mechanisms in diverging ecological adaptations. *Prog. Brain Res.* 195, 3–24 (2012).
23. Herculano-Houzel, S., Collins, C. E., Wong, P., Kaas, J. H. & Lent, R. The basic nonuniformity of the cerebral cortex. *Proc. Natl. Acad. Sci. U. S. A.* 105, 12593–12598 (2008).
24. Li, H. *et al.* Automated claustrum segmentation in human brain MRI using deep learning. *Hum. Brain Mapp.* 42, 5862–5872 (2021).
25. Ewert, S. *et al.* Toward defining deep brain stimulation targets in MNI space: A subcortical atlas based on multimodal MRI, histology and structural connectivity. *Neuroimage* 170, 271–282 (2018).
26. Horn, A. *et al.* Lead-DBS v2: Towards a comprehensive pipeline for deep brain stimulation imaging. *Neuroimage* 184, 293–316 (2019).
27. Dong, H. W. The Allen reference atlas: A digital color brain atlas of the C57Bl/6J male mouse. 57B, 6J (2008).
28. Xu, N. *et al.* Functional connectivity of the brain across rodents and humans. *Front. Neurosci.* 16, 816331 (2022).
29. Krubitzer, L. The organization of neocortex in mammals: are species differences really so different? *Trends in neurosciences* 18, 408–417 (1995).
30. Johnson, G. A. *et al.* Merged magnetic resonance and light sheet microscopy of the whole mouse brain. *Proc. Natl. Acad. Sci. U. S. A.* 120, e2218617120 (2023).
31. Xiao, J. *et al.* A time-course study of actively stained mouse brains: Diffusion tensor imaging parameters and connectomic stability over 1 year. *NMR Biomed.* 35, e4611 (2022).
32. Lustig, M., Donoho, D. & Pauly, J. M. Sparse MRI: The application of compressed sensing for rapid MR imaging. *Magn. Reson. Med.* 58, 1182–1195 (2007).
33. Wang, N. *et al.* Whole mouse brain structural connectomics using magnetic resonance histology. *Brain Struct. Funct.* 223, 4323–4335 (2018).
34. Uecker, M. *et al.* Berkeley Advanced Reconstruction Toolbox. *Proceedings of the International Society for Magnetic Resonance in Medicine* 23, (2015).
35. Tustison, N. J. *et al.* Large-scale evaluation of ANTs and FreeSurfer cortical thickness measurements. *Neuroimage* 99, 166–179 (2014).
36. Anderson, R. J. *et al.* Small animal multivariate brain analysis (SAMBA) - a high throughput pipeline with a validation framework. *Neuroinformatics* 17, 451–472 (2019).
37. Hata, J., Nakae, K., Yoshimaru, D. & Okano, H. Brain/MINDS Marmoset Brain MRI Dataset NA216 (In Vivo) and eNA91 (Ex Vivo). Connectome Analysis Unit, Integrative Computational Brain Science Collaboration Division, RIKEN Center for Brain Science https://doi.org/10.24475/bminds.mri.thj.4624 (2022).
38. Milham, M. P. *et al.* An open resource for non-human primate imaging. *Neuron* 100, 61-74.e2 (2018).
39. Yeh, F.-C. Brain MRI segmentation using template-based training and visual perception augmentation. *ArXiv* (2023).
40. Yeh, F.-C. DSI Studio: an integrated tractography platform and fiber data hub for accelerating brain research. *Nat. Methods* 22, 1617–1619 (2025).

41. Destrieux, C., Fischl, B., Dale, A. & Halgren, E. Automatic parcellation of human cortical gyri and sulci using standard anatomical nomenclature. *Neuroimage* 53, 1–15 (2010).
42. Fischl, B. FreeSurfer. *Neuroimage* 62, 774–781 (2012).
43. Zilles, K. & Amunts, K. Centenary of Brodmann's map — conception and fate. *Nat. Rev. Neurosci.* 11, 139–145 (2010).
44. Calabrese, E. *et al.* A diffusion tensor MRI atlas of the postmortem rhesus macaque brain. *Neuroimage* 117, 408–416 (2015).
45. Rohlfing, T. *et al.* The INIA19 template and NeuroMaps atlas for primate brain image parcellation and spatial normalization. *Front. Neuroinform.* 6, 27 (2012).
46. Woodward, A. *et al.* The Brain/MINDS 3D digital marmoset brain atlas. *Sci Data* 5, 180009 (2018).
47. Liu, C. *et al.* A digital 3D atlas of the marmoset brain based on multi-modal MRI. *Neuroimage* 169, 106–116 (2018).
48. Majka, P. *et al.* Towards a comprehensive atlas of cortical connections in a primate brain: Mapping tracer injection studies of the common marmoset into a reference digital template. *J. Comp. Neurol.* 524, 2161–2181 (2016).
49. Nishio, N. *et al.* Higher visual responses in the temporal cortex of mice. *Sci. Rep.* 8, 11136 (2018).
50. Glickfeld, L. L. & Olsen, S. R. Higher-order areas of the mouse visual cortex. *Annu. Rev. Vis. Sci.* 3, 251–273 (2017).
51. Ranganath, C. & Ritchey, M. Two cortical systems for memory-guided behaviour. *Nat. Rev. Neurosci.* 13, 713–726 (2012).
52. Beaudin, S. A., Singh, T., Agster, K. L. & Burwell, R. D. Borders and Comparative Cytoarchitecture of the Perirhinal and Postrhinal Cortices in an F1 Hybrid Mouse. *Cereb. Cortex* 23, 460–476 (2013).
53. Zilles, K. & Amunts, K. Chapter 23 - Architecture of the Cerebral Cortex. in *The Human Nervous System (Third Edition)* (eds. Mai, J. K. & Paxinos, G.) 836–895 (Academic Press, San Diego, 2012).
54. van Heukelum, S. *et al.* Where is Cingulate Cortex? A Cross-Species View. *Trends Neurosci.* 43, 285–299 (2020).
55. Russo, M. J., Franks, K. M., Oghaz, R., Axel, R. & Siegelbaum, S. A. Synaptic organization of anterior olfactory nucleus inputs to piriform cortex. *J. Neurosci.* 40, 9414–9425 (2020).
56. Fahn, S., Jankovic, J. & Hallett, M. Functional neuroanatomy of the basal ganglia. in *Principles and Practice of Movement Disorders* 55–65 (Elsevier, 2011).